Chemical Engineering Science 65 (2010) 1345–1353

Contents lists available at ScienceDirect

Chemical Engineering Science

journal homepage: www.elsevier.com/locate/ces

Photocatalytic oxidation of oxalic acid in dilute aqueous solution, in a fully illuminated fluidized bed reactor

Roberto L. Pozzo *, Rodolfo J. Brandi, Alberto E. Cassano, Miguel A. Baltanás

Instituto de Desarrollo Tecnológico para la Industria Química (UNL – CONICET), Güemes 3450, (3000) Santa Fe, Argentina

ARTICLE INFO

Article history:
Received 26 December 2008
Received in revised form
8 July 2009
Accepted 6 October 2009
Available online 13 October 2009

Keywords:
Adsorption
Kinetics
Photochemistry
Mathematical modeling
Reaction engineering
Pollution
Fluidized bed
Reaction mechanism

ABSTRACT

A comprehensive kinetic model for the photooxidation of oxalic acid ($C_2O_4H_4$) in a fluidized bed (FB) of a TiO_2/quartz sand composite, in a UV-fully illuminated photoreactor, was developed and correlated with experimental results. A proper solution for the mass balance of the reacting system was achieved by combining the complete radiation field profile and the most recent and updated pathway for the adsorption and photodecomposition of oxalic acid onto TiO_2 (Mendive et al., 2007), which was employed to determine the kinetic expression and model parameters.

1. Introduction

The degradation of water pollutants by photo activated fluidized beds (FB) of a composite made of titanium dioxide supported on quartz sand is being systematically investigated by our group as an alternative to the slurried systems of finely powdered photocatalysts that, in most cases, require the additional cost of downstream separation steps. In both situations the description and evaluation of the radiation field inside the reaction volume is a prerequisite for achieving a significant kinetic modeling of the photocatalytic process and/or for reactor design purposes.

In a previous work (Pozzo et al., 2006), a methodological approach to determine the radiation field profile in a FB of the titania–quartz sand composite was presented. As a result, a functional dependency between the specific volumetric optical parameters (that is, the spectral absorption and scattering coefficients) with bed height was proposed and validated, by assuming a perfect size-classification model for the FB (viz.: only one particle size can exist at each FB level). Furthermore, the local volumetric rate of photon absorption (LVRPA) was calculated by solving the radiation transfer equation (RTE), using a two-dimensional (2D) model. The reacting system was a rectangular prismatic space confined between two parallel optical windows. The optical coefficients of differently expanded narrow-path FB of the same photocatalyst, at given pre-specified FB heights, were previously evaluated by means of a unidirectional and one-dimensional (1DD) model of the RTE (Pozzo et al., 2005).

Along these lines, a similar methodological approach was used in the present work, in order to assess its capability to model the intrinsic reaction kinetics of the photodecomposition of oxalic acid ($C_2O_4H_4$) inside a batch, recirculating photocatalytic FB reactor, because fluidized beds are well-known devices capable of minimizing mass-transfer limitations. Oxalic acid, a well-known by-product in the process of mineralization of many water pollutants, was chosen as a suitable model reactant, given its relatively simple decomposition chemistry (to CO_2) in an oxygenated solution, without lasting intermediates.

The experimental reactor design of our former set up (namely: a fully illuminated FB photoreactor with a well-characterized LVRPA field) was kept. Yet, because of the low initial concentrations of oxalic acid that were employed, 10–40 ppm (i.e. under the saturation range of titania, Pozzo et al., 2006), the concentration profiles in the reactor had to be modeled as dependent on both time and reactor height.

The most recent and updated pathway for the adsorption and photodecomposition of oxalic acid onto titanium dioxide, presented by Mendive et al. (2006, 2007), was adopted as the basic mechanistic scheme to determine a kinetic expression useful for modeling purposes.

* Corresponding author. Fax: +54 342 455 9175.
E-mail address: rpozzo@intec.santafe-conicet.gov.ar (R.L. Pozzo).

0009-2509/$ - see front matter © 2009 Elsevier Ltd. All rights reserved.
doi:10.1016/j.ces.2009.10.002

2. Experimental set up

All the experiments were carried out by using a slender planar reactor/cell with a 7.0 mm optical gap constituted by a pair of optically clear 3.0 mm thick Tempax® borosilicate glass walls, each one respectively attached to both sides of a hollow frame of aluminum. The cell was horizontally divided into two compartments by a Teflon® mesh, and a fluidized bed of the TiO_2–quartz sand catalyst composite was allowed to develop in the 21 cm high upper one, while the lower space was filled with glass spheres (dia.=2 mm) for reducing jet formation in the bed zone immediately above the mesh. A bed of 20 g of the catalytic composite was expanded seven times its unexpanded volume in all the tested oxalic solutions. A schematic representation of the reactor is shown in Fig. 1. For each run, fresh aliquots of the catalyst stock were used. A constant hydrostatic pressure generation device was used to stabilize the FB, by maintaining a relatively high liquid flow rate of about 2.2 $cm^3 s^{-1}$. This device consisted of two 'open-atmosphere' recirculating loops that included two reservoir tanks, labeled as tank 2 (80 cm^3) and tank 3 (200 cm^3) in Fig. 1. Mechanical agitation in the bigger reservoir tank assured a uniform concentration of the solute (oxalic acid) in the recirculating system, outside the reactor cell. A constant concentration of dissolved O_2 was achieved by air bubbling throughout each experimental run. Additional information about the FB recirculating system is given in a previous work (Pozzo et al., 2005).

A pair of tubular black light lamps (Philips TLD 18W/08; nominal output power: 18 W; superficial emission from 340 to 400 nm, with a peak at 365 nm) was employed as the UV irradiation system. The lamps were situated lengthwise, one at each side of the cell, concurrent with the focal axis of two parabolic reflectors made of an aluminum sheet, specularly finished (Alzac treated) to concentrate the rays (Fig. 1). Within the lamp radiation spectral span, the calculated *specific* scattering and absorption coefficients were practically constant; i.e.: the FB behaves practically as a gray body with respect to both parameters (Pozzo et al., 2005). In this way, both reactor windows were 'quasi uniformly' irradiated. The incident radiation power from each lamp to the reactor windows was determined via actinometry by recirculating a 6×10^{-6} mol cm^{-3} solution of potassium ferrioxalate through the reaction space. More details on these actinometric determination procedures can be found in a previous report of some of us (Pozzo et al., 1999).

The catalyst composite was prepared by low-temperature CVD-plasma coating of Aldrich white quartz sand [Cat. no. 27,473-9, Lot no. 06313JN]; ρ_s=2.4 g cm^{-3}; D_p=250 μm (+50–70 mesh) with a thin, compact film of TiO_2 (by using Ti *t*-butoxide as precursor) in a vacuum-operated circulating fluidized bed reactor. Detailed information about the preparation method and catalyst characterization is given elsewhere (Morstein et al., 2002). The TiO_2 loading was determined by dissolving the films in a 10 wt% solution of $(NH_4)_2SO_4$ in concentrated H_2SO_4 and subsequent quantification by elemental analysis.

A 2020*i* model Dionex ion chromatograph equipped with an AS4A-SC analytic column was used to monitor the photocatalytic degradation of oxalic acid (Carlo Erba RSE, 99.9%) in highly dilute aqueous solutions, which were prepared using nominal concentrations of $C_2O_4H_4$ equal to 4.9, 2.1 and 1.1×10^{-7} g mol cm^{-3} (45, 20 and 10 ppm, respectively) in ultra pure water. Triplicate runs were made for each nominal concentration. The precision of ion chromatography for this concentration level is 3–5%; all determinations were made in triplicates and averaged. The initial pH of the solutions, naturally determined by the corresponding oxalic acid concentration, was 3.5 ± 0.1). Steady state temperature and lamp operation conditions were set prior to initiating any experimental run.

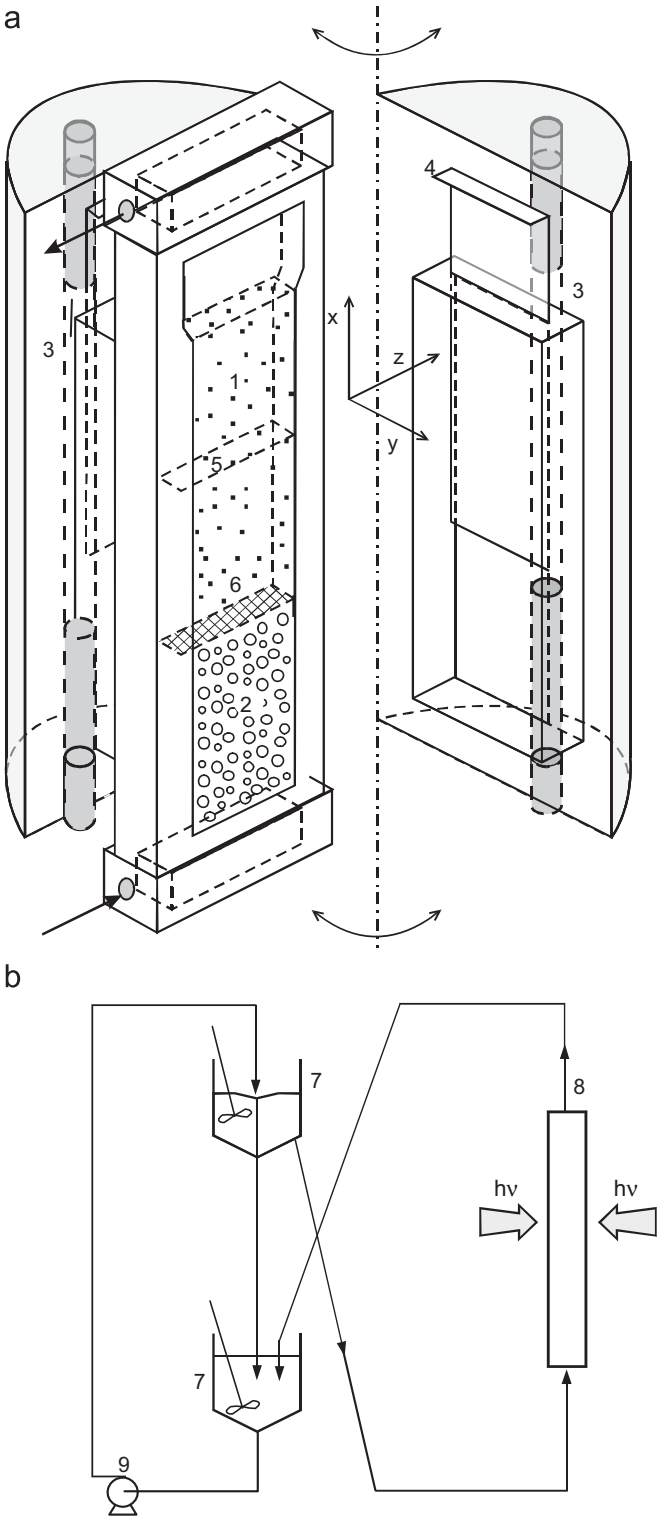

Fig. 1. (a) Plane photoreactor: (1) FB compartment, (2) glass beads compartment, (3) lamp-reflector illumination device, (4) sliding hatch, (5) FB transversal area, and (6) Teflon® mesh. (b) Experimental set-up: (7) reservoir tank, (8) photoreactor, and (9) peristaltic pump.

3. Local electron–hole generation rate and FB features

An efficient activation of electron–hole pairs on the catalyst surface is the key step in any photocatalytic reaction. Its local generation rate, $r_g(\underline{x})$, is directly proportional to the catalyst

radiation absorption efficiency, which is a convoluted function of the *spectral* local volumetric rate of photon absorption, $e^a_\lambda(\underline{x})$, and the *spectral* quantum yield, Φ_λ, of the photocatalyst. In practice, it is generally assumed (Alfano et al., 1997; Imoberdorf et al., 2007) that

$$r_g(\underline{x}) = \overline{\Phi}\sum_\lambda e^a_\lambda(\underline{x}) = \overline{\Phi} e^a(\underline{x}) \quad (1)$$

where $\overline{\Phi}$ is a special wavelength averaged primary quantum yield, representing the yield of separated carriers reaching the catalytic surface, excluding the external surface recombination rate, and $e^a(\underline{x})$ is the local volumetric rate of photon absorption (from now on, LVRPA).

To evaluate the LVRPA, it is necessary to model the radiation field in the entire reaction volume. Thus, the unavoidable segregation suffered by the particles of the photocatalyst composite (which have a given size distribution) must be taken into account. First of all, as already shown in a previous work (Pozzo et al., 2006), the local optical properties of the FB become affected by axial changes in the solid hold-up because, as the voidage of the fluidized bed steadily increases toward the upper zone (where the smaller particles predominate), the light energy is then able to penetrate further (low volumetric extinction). Conversely, in the lower region of the FB, featuring a smaller bed voidage and a higher concentration of coarser particles, the light extinction intensifies, so that the penetration depth of the radiation is much smaller. Likewise, the local volumetric concentration of the active catalyst (TiO_2) also depends on the particle size distribution of the composite and, consequently, is a function of bed height as well.

With our experimental set up, it can be expected that the radiation field will strongly vary both vertically along the FB (x direction), due to 'particle-size-distribution related' anisotropy, and transversally (y direction), because of the radiation extinction through the thickness of the reaction volume. By design, due to the uniformity of the incident radiation flux and assuming a negligible incidence of border effects, no significant changes would occur, instead, along the width (z direction, horizontal) of the reactor.

Briefly, by assuming a perfect size-classification model for the FB (viz.: only one particle size can exist at each FB level), the integro-differential radiation transfer equation (RTE), was solved and validated in a previous work (Pozzo et al., 2006). The corresponding $e^a(x, y)$, that is, the LVRPA at position x, y in the reactor (see Fig. 1) could be determined, by using the functional dependency upon bed height of both, the spectral optical coefficients of light absorption and scattering: $\kappa_\lambda(\underline{x})$ and $\sigma_\lambda(\underline{x})$, respectively, already established in an earlier investigation (Pozzo et al., 2005).

By assuming that complete lateral mixing is achieved in this segregated FB, a one-dimensional flow (in the x direction) would suffice to write the mass balance of oxalic acid inside the reaction volume (see below). Therefore, to assess the impact of particle segregation on photon availability along the FB, area-averaged values of the square root of LVRPA, $\langle [e^a(x,y)]^{1/2} \rangle$, were calculated by averaging $\sqrt{e^a(\underline{x})}$ through the transversal area (A_T) at each axial position, x, of the reactor height. These area-averaged values are depicted in Fig. 2, together with the FB voidage, ε_h, and the particle size, D_p, as a function of FB height.

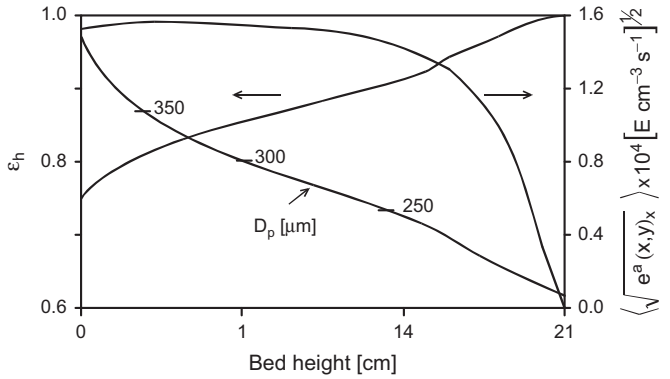

Fig. 2. Values of $\langle \sqrt{e^a(x,y)} \rangle$, ε_h, and D_p as a function of FB height (x) (from Pozzo et al., 2006).

4. About the kinetic model

Several kinetic models have been proposed for the heterogeneous photocatalytic mineralization of organic water contaminants. The key step involves the photogeneration of hole–electron pairs in the catalyst particle (usually TiO_2), which migrate to the surface, thus giving place to a competition between their recombination versus the interfacial charge transfer to adsorbed species: electron donors for the holes (oxidation process) and electron acceptors for the electrons (reduction process). In natural waters, there is general consensus in that oxygen is the main electron acceptor. However it is still a matter of debate whether the oxidation process proceeds via $OH^\cdot$ radicals, after hole trapping of OH^- or water molecules (Kosanić, 1998), or via direct hole transfer to an adsorbed reductant (Krýsa et al., 2006; Bahnemann et al., 1997; Bahnemann, 1999; Zalazar et al., 2005).

Mao et al. (1991), by using a combination of photocatalytic and radiation chemistry studies, showed that the OH^- channel appears to be the favored reaction path for the photodegradation of halogenated organic compounds. On the other hand, they found that the oxidation of carboxylic acids, in particular of oxalic acid, proceeds primarily via direct hole trapping (photo-Kolbe type of reaction mechanism), in agreement with some other workers (Choi and Hoffmann, 1995; Peill and Hoffman, 1996).

As regards the adsorption processes of $C_2O_4H_4$, a Langmuir–Hinshelwood type of pattern was put forward in earlier reports, by assuming a single and uniform Langmuirian adsorption of the dicarboxylic acid (Matthews, 1987; Al-Ekabi and Serpone, 1988; Sabate et al., 1991). However, it was not still clear whether radiation affected adsorption and, therefore, photoadsorption phenomena were—in general—ignored as likely or significant factors in their proposed reaction mechanisms.

More recent research showed that, at least in the case of oxalic acid, things were somewhat more intricate. For instance, Jiang et al. (2004), by using a transient photoelectrolytic technique, were able to reveal the formation of three thermodynamically distinct types of oxalic acid complexes on the TiO_2 surface and—at least—two different decomposition kinetic regimes, one clearly faster than the other. In correspondence with these findings, 10 years earlier Hug and Sulzberger (1994) had already found by using FTIR-ATR spectroscopy that sulfates, acetates, and oxalates, adsorb as a variety of surface complexes on TiO_2 (Degussa P-25, mostly anatase).

At similar conclusions arrived Weisz et al. (2001), Mendive et al. (2005) and Araujo et al. (2005) in a series of systematic works devoted to the analyses of the heterogeneous photocatalytic oxidation of salicylic and oxalic acids and their salts on the surface of TiO_2, and characterization of the reaction intermediates, using FTIR spectroscopy. Some of them also reported a transient redistribution of adsorbed oxalate complexes on the titania surface upon UV irradiation (Mendive et al., 2006, 2007). Essentially, what they claim is that in aqueous solution the oxalate ions reach adsorption equilibrium with TiO_2 in the form of two kinds of surface complexes: a more stable bidentate structure

(named species A hereafter) and a more labile one (named species B hereafter), with the sigma carbon–carbon bond either parallel or perpendicular to the TiO_2 surface, respectively. Lastly, in what perhaps was their most significant finding, they also were able to show that, upon illumination, the adsorption equilibriums were modified in such a way that the surface coverage of TiO_2 by species B declined with time, whereas the area occupied by species A incremented, instead.

According to these authors, this substitution process would be favored by the photodegradation of the sterically more exposed species B. Even more, they put forward that species B would be readily attacked, via a faster $OH^{\cdot}$ mechanism**,** as compared to the sluggish direct hole transfer oxidation process for species A, an inner-sphere complex in intimate contact with the TiO_2 surface.

This mechanistic scheme proposed by Mendive et al., characterized by two parallel, simultaneous kinetic pathways, emerged as the most promising to model our results for the photodegradation of oxalic acid on the quartz-supported TiO_2 photocatalyst and, therefore, it was adopted in the present work. An outline of the complete reaction scheme including both, the fast reaction pathway (via $OH^{\cdot}$ attack) and the slower one (via direct hole-transfer) is detailed in Table 1.

5. Results and discussion

5.1. Experimental results. Preliminary analysis

The time-evolution of the oxalate ion concentrations, referred to the initial values ($[Ox^-]_{sol}/[Ox^-]^0_{sol}$), are depicted in Fig. 3, for $[Ox^-]^0_{sol} = 10$, 20, and 40 ppm, respectively. It is apparent, from the mere observation of these concentration profiles, that associating a simple Langmuir–Hinshelwood type of kinetics to the photocatalytic decomposition of oxalic acid is impracticable. Rather, two different tendencies can be clearly observed in all three cases: an initial, relatively faster temporal evolution followed by a clear-cut slowing down of the reaction.

This 'progressive-freezing' effect over the reaction cannot be assigned to external or internal mass transfer limitations inside the photocatalytic reactor, as the dynamic conditions of the fluidized bed grant an estimated liquid–solid mass transfer coefficient of about $2.6 \times 10^{-2}\,cm\,s^{-1}$ (Nikov and Karamazov, 1991) and the compactness of the plasma-deposited titania onto the quartz sand was explicitly verified (Morstein et al., 2002) excluding, consequently, internal limitations. It can be observed in Fig. 3, also, that the slowing down of the reaction did not occur at a similar reaction time for all the conditions: it came about later, the higher the initial oxalic concentration was.

Certainly, an initial zero order reaction rate with respect to $[Ox^-]_{sol}$ is not appreciable from our experimental data (in such a case, the higher the initial concentration were made the slower the time-evolution would be, which is exactly the opposite to the

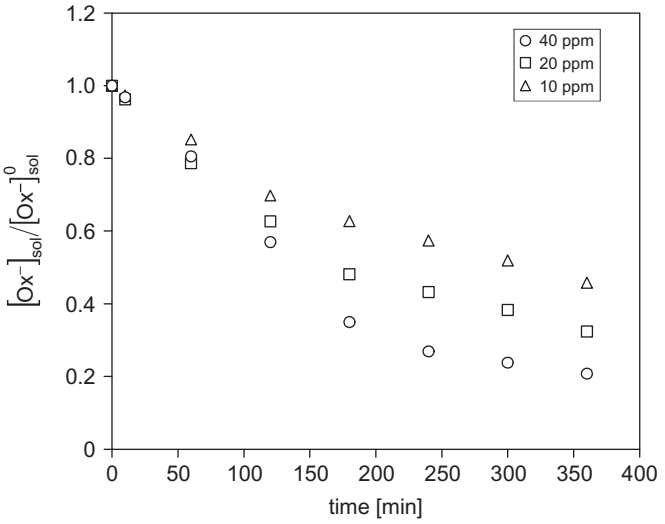

Fig. 3. Oxalate ion concentrations, referred to initial values (40, 20 and 10 ppm), vs. reaction time.

Table 1
Reaction scheme for the heterogeneous photodecomposition of oxalic acid on TiO_2.

Reaction step	Equilibrium constant	Reaction rate code	Kinetic rate constant	Reaction step Nbr
Activation (common to both pathways)				
$TiO_2 \xrightarrow{h\upsilon} h^+ + e^-$		r_g		(S_0)
Adsorption (species A) on dark/illumination conditions				
$[site] + C_2O_4H^-_{(sol)} \leftrightarrow C_2O_4H^-_{(ads)A}$	K^0_A/K_A	r^0_1/r_1		(S_1)
Adsorption (species B) on dark/illumination conditions				
$[site] + C_2O_4H^-_{(sol)} \leftrightarrow C_2O_4H^-_{(ads)B}$	K^0_B/K_B	r^0_2/r_2		(S_2)
Adsorption of oxygen				
$[site] + O_{2(sol)} \leftrightarrow O_{2(ads)}$	K_3	r_3		(S_3)
Hole trapping (via $OH^{\cdot}$) and σ bond rupture (fast kinetics)				
$(OH^-)_{ads} + h^+ \leftrightarrow OH^{\cdot}$		r_4	k_4, $k_{4\_}$	(S_4)
$C_2O_4H^-_{(ads)B} + OH^{\cdot} \rightarrow CO_2H^{\cdot}_{(ads)B} + CO_2 + OH^-$		r_5	k_5	(S_5)
Hole trapping (direct) and σ bond rupture (slow kinetics)				
$C_2O_4H^-_{(ads)A} + h^+ \rightarrow CO_2H^{\cdot}_{(ads)A} + CO_2$		r_6	k_6	(S_6)
Final mineralization (common to both mechanisms)				
$C_2O_4H^{\cdot}_{(ads)} + O_2 \rightarrow O_2H^{\cdot} + CO_2$		r_7	k_7	(S_7)
Electron capture				
$O_{2(ads)} + e^- \rightarrow O^{\cdot-}_{2(ads)}$		r_8	k_8	(S_8)
Hole–electron recombination				
$e^- + h^+ \rightarrow$ heat		r_9	k_9	(S_9)
Complementary (assumed fast) reactions				
$O^{\cdot-}_{2(ads)\ (ads)} + H^+ \rightarrow O_2H^{\cdot}$				
$2O_2H^{\cdot} \rightarrow H_2O_2 + H_2O$				
$H_2O_2 \rightarrow H_2O + O_2$				

After Mendive et al. (2005, 2006, 2007).

observed behavior, nor a first order kinetics (well-suited to an oxidation mechanism via hydroxyl radicals) is perceived. In such a case, the same time evolution of the non-dimensional concentration of oxalic acid, ($[Ox^-]_{sol}/[Ox^-]^0_{sol}$) would be obtained which, again, is not in agreement with the experimental observations. Likewise, a square root time-dependence of the oxalic concentration (obtained by a simple regression of the raw data), which is compatible with a direct hole transfer as the determining mechanism step, did not qualify as a good representative of the photoreaction for the complete time span.

5.2. The kinetic equation

In view of the foregoing discussion, it is evident that a more complex pathway than such as those based on a single Langmuirian-type of adsorption site on the catalyst surface, needs to be postulated to properly model the observed reaction kinetics. An alternative option emerges by taking into account the mechanistic implications of the reaction scheme put forward by Mendive et al. (2006, 2007), which considers the titania surface consisting of two well differentiated areas, with different adsorptive and (photo)-catalytic properties, where oxalate ions adsorb on TiO_2 as two kinds of surface complexes (already presented as species A and B in the 'About the kinetic model' section of the present work).

On the basis of said reaction scheme, the following assumptions were made in the present investigation to obtain an expression of the local (intrinsic), overall reaction rate inside the photocatalytic reactor: (1) hole trapping by adsorbed oxalic acid (reaction 4) and bond rupture by $OH^{\cdot}$ (reaction 6) are believed to be the rate controlling steps in the slow and in the fast kinetic pathways, respectively (Turchi and Ollis, 1990); (2) a Langmuirian type of adsorption equilibrium is assumed for both species A and B, either under dark or illuminated conditions; (3) in the dark, the areal fraction of the titania surface occupied by species B, at equilibrium, is assumed to be proportional (quasi-linear zone of the adsorption isotherm of species B) to the concentration of oxalic acid in the aqueous phase, while the area occupied by species A is considered as independent of said concentration (saturation zone of species A isotherm), respectively. Also, according to Hug and Sulzberger (1994), $K^0_A \gg K^0_B$ for the whole range of oxalic acid concentration used in the present work; (4) as the fraction of the catalyst surface occupied by species B diminishes along the photooxidation process, the spaces left are re-occupied by species A (the species being photo-oxidized at a slower rate), thus maintaining approximately constant the total catalyst area occupied by adsorbed oxalate species. (In what follows it will be also assumed, as a first approximation, that the decreasing occupation of the TiO_2 surface by species B is a linear function of time and the LVRPA.); (5) the concentration of adsorbed oxygen on the titania surface is taken as proportional to the concentration of oxygen in the solution (Zalazar et al., 2005), which was kept constant in all the experimental runs by bubbling air into the aqueous solution; (6) also, and according to Blanco et al. (2001) it can be postulated that oxygen adsorbs in different sites than oxalate ions do; (7) the steady state approximation may be applied for unstable reaction intermediates such as hydroxyl and other radicals, electrons and semiconductor holes, (8) the local generation rate of the hole–electron pairs, r_g, can be adequately established by the 2D radiation field modeling in the FB given by Pozzo et al. (2006), as briefly outlined above.

Thence, according to the reaction scheme and the above-mentioned assumptions, it is possible to arrive at the following general expression for the local, overall reaction rate at each axial position (x) of the reactor height, as a function of the local electron–hole generation rate ($r_g(\underline{x})$), the concentration of relevant adsorbed reactants on the catalyst surface, the local mean particle diameter (D_p), and the local fluidized bed voidage (ε_h) as it is shown in detail in Appendix A (Eq. (A.33)):

$$r_{ox}(\underline{x},t)=\frac{k_B\theta(t)[Ox^-]_B\overline{\Phi}e^a(\underline{x})}{\frac{1}{2}+\sqrt{\frac{1}{4}+\frac{k'_B\,D_p\overline{\Phi}e^a(\underline{x})}{\phi'(1-\varepsilon_h)[O_2]_{ads}}}}+\frac{[1-\theta(t)]\overline{\Phi}e^a(\underline{x})}{\frac{1}{2}+\sqrt{\frac{1}{4}+\frac{D_pk_A\overline{\Phi}e^a(\underline{x})}{\phi'(1-\varepsilon_h)[O_2]_{ads}[Ox^-]_A}}} \tag{2}$$

By introducing assumption 2 (Langmuirian adsorption) for the reaction system under illumination and assumption 5 (partitioned adsorbed oxygen concentration), Eq. (2) can be rewritten as follows:

$$r_{ox}(\underline{x},t)=\frac{k_B\theta(t)K_B[Ox^-]^{sat}_B[Ox^-]_{sol}\overline{\Phi}e^a(\underline{x})}{(1+K_B[Ox^-]_{sol})\left(\frac{1}{2}+\sqrt{\frac{1}{4}+\frac{k'_B\,D_p\overline{\Phi}e^a(\underline{x})}{\phi'(1-\varepsilon_h)K_3[O_2]_{sol}}}\right)}+\frac{[1-\theta(t)]\overline{\Phi}e^a(\underline{x})}{\frac{1}{2}+\sqrt{\frac{1}{4}+\frac{D_pk_A(1+K_A[Ox^-]_{sol})\overline{\Phi}e^a(\underline{x})}{\phi'(1-\varepsilon_h)K_3[O_2]_{sol}K_A[Ox^-]^{sat}_A[Ox^-]_{sol}}}} \tag{3}$$

where $\theta(t)=\beta[Ox^-]^0_{sol}[1-\alpha e^a(\underline{x})t]$ (see Eq. (A.4) in Appendix A).

To ease the kinetic analysis, the following bounding conditions are assumed (Hug and Sulzberger, 1994; Pozzo et al., 2006):

(1) $\dfrac{k_BD_p\overline{\Phi}e^a(\underline{x})}{\phi'(1-\varepsilon_h)K_3[O_2]_{sol}}\geqslant 0.25$

(2) $\sqrt{\dfrac{1}{4}+\dfrac{k'_B\,D_p\overline{\Phi}e^a(\underline{x})}{\phi'(1-\varepsilon_h)K_3[O_2]_{sol}}}\geqslant 0.5$

(3) $\dfrac{D_pk_A(1+K_A[Ox^-]_{sol})\overline{\Phi}e^a(\underline{x})}{\phi'(1-\varepsilon_h)K_3[O_2]_{sol}K_A[Ox^-]^{sat}_A[Ox^-]_{sol}}\geqslant 0.25$

(4) $\sqrt{\dfrac{1}{4}+\dfrac{D_pk_A(1+K_A[Ox^-]_{sol})\overline{\Phi}e^a(\underline{x})}{\phi'(1-\varepsilon_h)K_3[O_2]_{sol}K_A[Ox^-]^{sat}_A[Ox^-]_{sol}}}\geqslant 0.5$

(5) $K_B[Ox^-]_{sol}\ll 1$

(6) $K_A[Ox^-]_{sol}\ll 1$

Then, the following simplified expression for the local, overall reaction rate is obtained:

$$r_{ox}(\underline{x},t)=\left\{k^{obs}_B\theta(t)[Ox^{-1}]_{sol}+k^{obs}_A[1-\theta(t)]\sqrt{[Ox^-]_{sol}}\right\}\sqrt{\frac{(1-\varepsilon_h)e^a(\underline{x})}{D_P}} \tag{4}$$

where

$$k^{obs}_B=\frac{k_BK_B[Ox^-]^{sat}_B}{\sqrt{k'_B}}\sqrt{\phi'\overline{\Phi}K_3[O_2]_{sol}}$$

and

$$k^{obs}_A=\sqrt{\frac{\phi'\overline{\Phi}(K_A[Ox^-]^{sat}_AK_3[O_2]_{sol})}{k_A}}$$

From Eq. (4), it can be readily appreciated that the simplified final expression of the local overall reaction rate resembles the combined result of two mechanisms working in parallel from the beginning of the heterogeneous photocatalytic process: a first order kinetics, plus a square root kinetic dependence with respect to the oxalic acid concentration in solution, respectively. As the reaction time goes on, and $\theta(t)$ tends to zero, the second mechanism (governed by the square root dependence) takes progressive control of the process, until it prevails at the end. Interestingly, the characteristic square root dependence with respect to the LVRPA appears as common

to both mechanisms, which is typical of well-irradiated reacting systems.

5.3. The mass balance of the reaction system

The complete reaction system constitutes a closed recycling loop, between the FB photoreactor and the reservoir tank, of a dilute aqueous solution of oxalic acid. By design, the granular particles of the photocatalyst are not dragged outside the FB reactor, so that only the liquid phase enters the tank. Also, as the outflow concentration of oxalic acid from the reservoir tank becomes the ingoing concentration of the reactor, and vice versa, the mass balances of both components of the recycling loop are coupled.

The reservoir tank can be modeled as a perfectly mixed CSTR. Yet, because the inlet concentration of oxalic acid to the tank is continuously changing with time (permanent non-stationary state) a time-dependent, uniform concentration exits the tank volume as well. Under these assumptions, the mass balance for the oxalic acid in the reservoir tank can be written as

$$\frac{d[\mathrm{Ox}^-]_{Tk}^{\mathrm{out}}}{dt} = \frac{Q}{V_{Tk}}([\mathrm{Ox}^-]_{Tk}^{\mathrm{in}} - [\mathrm{Ox}^-]_{Tk}^{\mathrm{out}}) \tag{5}$$

where $[\mathrm{Ox}^-]_{Tk}^{\mathrm{out}}\,(t=0) = [\mathrm{Ox}^-]_{\mathrm{sol}}^0$, Q is the recirculating liquid flow, V_{Tk} is the reservoir tank volume $[\mathrm{Ox}^-]_{Tk}^{\mathrm{out}}$ and $[\mathrm{Ox}^-]_{Tk}^{\mathrm{in}}$ are the outflow and inflow oxalic acid concentrations, respectively.

As a fairly uniform liquid flow could be achieved using the Teflon® separator/flow distributor mesh, and $\sqrt{e^a(\underline{x})}$ was superficially averaged, a one-dimensional flow (in the x direction) suffices to write the mass balance of oxalic acid inside the reaction volume. That is, the vertical variations in concentration are regarded as more significant as compared to the lateral ones. Also, because the FB operates under steady-state flow conditions, the bed voidage is not a function of time but only a function of the coordinate. Likewise, the superficial velocity, U_0, can be supposed as uniform because of the continuity equation. With these hypotheses, the mass balance in the reactor can be written as

$$\varepsilon_h \frac{\partial[\mathrm{Ox}^-]_R}{\partial t} + U_0 \frac{\partial[\mathrm{Ox}^-]_R}{\partial x} = \langle r_{\mathrm{ox}}(x,y)\rangle_{\mathrm{A}_T}|_t \tag{6}$$

where

$$\langle r_{\mathrm{ox}}(x,y)\rangle|_t = \langle r_{\mathrm{ox}}(x,y)\rangle_{\mathrm{A}_T}|_t = \frac{1}{\mathrm{A}_T}\int_{\mathrm{A}_T} r_{\mathrm{ox}}(\underline{x},t)\,dy\,dz \tag{7}$$

$$[\mathrm{Ox}^-]_R(x=0,t) = [\mathrm{Ox}^-]_R^{\mathrm{in}}(t) = [\mathrm{Ox}^-]_{Tk}^{\mathrm{out}}(t) \tag{8}$$

and

$$[\mathrm{Ox}^-]_R(x,t=0) = [\mathrm{Ox}^-]_R^0(x) = [\mathrm{Ox}^-]_{\mathrm{sol}}^0 \tag{9}$$

The temporal derivative can be approximated by using a finite difference method. Thus, the mass balance becomes an ordinary differential equation, which must be solved progressively using small time increments, as follows:

$$U_0\frac{d[\mathrm{Ox}^-]_R}{dx}\bigg|_{t_i} = \langle r_{\mathrm{ox}}(x,y)\rangle\bigg|_{t_i} - \varepsilon_h\frac{[\mathrm{Ox}^-]_R(x,t_i) - [\mathrm{Ox}^-]_R(x,t_i-\Delta t)}{\Delta t} \tag{10}$$

where

$$[\mathrm{Ox}^-]_R(x=0,t=t_i) = [\mathrm{Ox}^-]_{Tk}^{\mathrm{out}}(t=t_i)$$

and

$$[\mathrm{Ox}^-]_R(x,t=0) = [\mathrm{Ox}^-]_{\mathrm{sol}}^0 \tag{11}$$

The system of equations is completed by using the expression for the local, overall reaction rate given by Eq. (4) (averaged in A_T as per Eq. (6)), which is a function of both, the FB height and the elapsed time (see Appendix A). It was numerically solved by following the calculation procedure described in Appendix B.

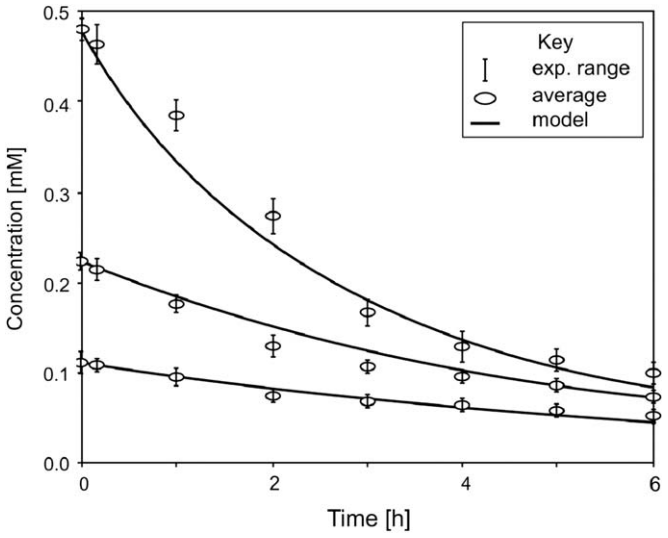

Fig. 4. Oxalate ion concentration vs. time, at the three initial concentrations tested.

5.4. Estimation of kinetic parameters

To estimate the kinetic parameters of the model, a modified Levenberg–Marquardt method was employed. This non-linear optimization algorithm allows estimating the parameter values that minimizes the sum of quadratic differences between the model-predicted concentrations vs. the experimental data.

The model predictions for the time evolution of the $C_2O_4H_4$ concentration are presented in Fig. 4 (solid lines), together with the corresponding experimental data, for the three initial concentrations that were tested. The root mean square error (RMSE) of the estimation was 8%. A fair agreement between computational results and experimental values can be observed in every case. This agreement between experimental data and model predictions, attained by combining two well-differentiated approaches (the first one, mainly based on FTIR spectroscopy of surface species, and the present one, supported on rigorous photoreactor engineering using a fully illuminated FB reactor,) strongly indicates that the surface-transient kinetic model based upon two well-differentiated adsorption sites is most appropriate to model the photocatalytic oxidation of oxalic acid on TiO_2. It also offers a promising approach to account for the observed photoreactivity of other adsorbed substrates featuring dicarboxylic acid groups, such as fulvic or humic acids.

The mean values for the relevant kinetics parameters obtained by means of the NLLS regression routine, together with their corresponding 95% confidence interval, are given in Table 2. As it can be readily appreciated, the fast kinetic rate constant ($k_{\mathrm{B}}^{\mathrm{obs}}$) is almost three orders of magnitude bigger than the slow kinetic rate constant ($k_{\mathrm{A}}^{\mathrm{obs}}$), which is consistent with the notorious differences in the reaction rates observed at the beginning of the photodegradation process, as compared to the ones observed at further reaction times.

6. Conclusions

By adopting a reaction mechanism based on the dual-site adsorption scheme proposed by Mendive et al. (2006, 2007) a new reaction kinetic model for the photocatalytic oxidation of oxalic

Table 2
Numeric values for the kinetic parameters.

Kinetic parameter	k_B^{Obs}	k_A^{Obs}	α	β
Units	$m^3\,mol^{-1}\,s$	$m^3\,mol^{-1}\,s$	$Einstein^{-1}\,m^3$	$cm^3\,mol^{-1}$
Parameter value	$(3.06\pm0.54)\times10^{-5}$	$(1.45\pm0.30)\times10^{-10}$	$(1.9\pm0.9)\times10^{-3}$	$(1.6\pm0.6)\times10^{-1}$

acid in dilute aqueous solutions using TiO_2/quartz sand, was proposed and successfully correlated with experimental data. A rigorous treatment of the radiation field inside a fully illuminated fluidized bed of the photocatalytic composite and of the mass balance of reaction system was employed. To accomplish these goals, former data regarding the relevant optical properties of the photocatalytic composite, as well as the fluid dynamics of the segregated fluidized bed were employed. The relevant kinetic constants were thus estimated.

Briefly, the overall reaction rate can be thought of as a combination of two pathways working in parallel, each one associated to a different adsorptive fraction of the TiO_2 surface, characterized by the following observable kinetic regimes: A relatively faster first order kinetics with respect to $[Ox^-]_{sol}$, associated with hole trapping, via $OH^{\cdot}$, by more labile adsorbed oxalate ions, and a slower square root dependence with $[Ox^-]_{sol}$, in which direct hole trapping by more stable adsorbed oxalate ions prevail. As the reaction progresses, though, a progressive substitution of the surface concentration of reactive, labile oxalate ions sets in so that a just a square root dependency is observable at longer reaction time.

Notation

D_p nominal mean particle diameter, μm
e^a local volumetric rate of radiative energy absorption, $Einstein\,m^{-3}\,s^{-1}$
h^+ semiconductor valence band hole
k reaction rate constant, units depends on the considered step
K equilibrium adsorption constant, $m^3\,mol^{-1}$
Ox^- oxalate ion
Q circulating liquid flow rate, $m^3\,s^{-1}$
r_g rate of electron-hole generation, $mol\,s^{-1}$
r_{ox} reaction rate, $mol\,s^{-1}$
S_v specific volumetric area, $m^2\,m^{-3}$
t time, s
U_0 superficial velocity, $m\,s^{-1}$
V volume, m^3
W_c local catalyst concentration, $g\,m^{-3}$

Greek letters

α constant, $Einstein\,m^{-3}$
β constant, $m^3\,mol^{-1}$
ε_h fluidized bed voidage, dimensionless
θ fraction of the catalyst surface occupied by species B
λ wavelength, nm
ρ_s quartz sand density, $g\,cm^{-3}$
Φ quantum yield, $mol\,Einstein^{-1}$
φ sphericity factor, dimensionless

Subscripts and superscripts

0 indicates initial time value
A, B indicates type of adsorbed species
obs refers to the observed kinetic constant
R refers to the FB reactor
sol indicates species in solution
Tk refers to the reservoir tank
$\underline{x}$ indicates position in the x, y, z coordinates system
x, y, z directional coordinates

Special symbols

$\langle\ \rangle$ represents an averaged value over a reactor transversal area
[=] means has units of

Acknowledgments

The authors thank the financial support from the Consejo Nacional de Investigaciones Científicas y Técnicas (CONICET), Universidad Nacional del Litoral (UNL) and ANPCyT of Argentina. Thanks are also given to Eng. Claudia Romani and to José L. Giombi for their skilled technical assistance.

Appendix A. An expression of the reaction rate from the proposed kinetic mechanism

As already said in the main text, at least two different types of oxalate ions chemisorb onto the active sites of the TiO_2–quartz sand photocatalyst composite, as oxalate complexes: type A (sigma–sigma carbon bond of the oxalate ion parallel to the catalyst surface, associated to a slow kinetics) and type B (sigma–sigma carbon bond perpendicular to the catalyst surface, associated to a fast kinetics), their interconversion being negligibly slow, as per Mendive et al. (2006, 2007). Therefore, for modeling purposes the photocatalyst can be virtually conceived as two inter-related ones working in parallel via its corresponding fraction of the catalyst active surface, each one with its specific physicochemical and catalytic properties. This would imply, for instance, that the adsorbed surface concentrations at equilibrium for each of the A and B oxalate types (either at dark or under illumination) might not be the same on each type of adsorbing sites, although their total surface concentration remains approximately constant. With this image in mind and the reaction scheme presented in Table 1, a general expression for the overall (intrinsic), local reaction rate can be written as follows:

$$r_{ox} = k_5\theta(t)[Ox^-]_B[OH^{\cdot}]_B + k_6[1-\theta(t)][Ox^-]_A[h^+]_A \quad (A.1)$$

where $\theta(t)$ stands for the fraction of the catalyst surface that is able to produce type B sites and the sub indices (A) and (B) stand for the surface concentrations of the referred, adsorbed reactants on type A or type B sites, respectively.

According to the kinetic model outlined in the main text, the declining evolution of the concentration fraction of type B sites is assumed (as a first approximation) as a decreasing linear function of the elapsed reaction time (t) from its dark value, θ_B^0 (i.e., the initial concentration, at t=0), with a slope proportional, by a factor α, to the LVRPA:

$$\theta(t) = \theta_B^0[1 - \alpha e^{a}(\underline{x})t] \tag{A.2}$$

Pursuant to assumption (4), the initial concentration fraction of type B sites can be considered as a linear function of the initial (i.e., prior to illumination) oxalic acid concentration in the aqueous solution:

$$\theta_B^0 = \beta[Ox^-]_{sol}^0 \tag{A.3}$$

Now, by introducing θ_B^0 from (A.3) into (A.2), the following relationship is obtained:

$$\theta(t) = \beta[Ox^-]_{sol}^0[1 - \alpha e^{a}(\underline{x})t] \tag{A.4}$$

In addition, from Eqs. (S_5) and (S_6) in Table 1

$$r_{OH^\cdot} = k_4[OH^-]_{ads}[h^+]_B - k_4[OH^\cdot]_{ads} - k_5[Ox^-]_B[OH^\cdot]_{ads} \tag{A.5}$$

and, by using the steady-state approximation for $[OH^\cdot]$, we get

$$[OH^\cdot]_{ads} = \frac{k_4[OH^-]_{ads}[h^+]_B}{k_4 + k_5[Ox^-]_B} \tag{A.6}$$

Given the low concentrations of oxalic acid in the aqueous phase and assuming the surface concentration of bound OH^-, $[OH^-]_{ads}$, as nearly constant (Turchi and Ollis, 1990), Eq. (A.6) can be written as follows:

$$[OH^\cdot]_{ads} \cong \frac{k_4[OH^-]_{ads}}{k_{4\_}}[h^+]_B \tag{A.7}$$

The concentration of holes and electrons on type B sites can be obtained from their corresponding balances between generation and disappearing rates, according to the reaction scheme shown in Table 1 and by taking into account Eq. (A.7), as follows:

$$r_{h^+} = r_g - k_4[OH^\cdot]_{ads}[h^+]_B - k_9[e^-][h^+]_B = k_4'[h^+]_B + k_9[e^-][h^+]$$

where

$$k_4' = \frac{(k_4)^2}{k_{4\_}}[OH^-]_{ads} \tag{A.8}$$

$$r_e = r_g - k_9[e^-][h^+]_B - k_8[O_2]_{ads}[e^-] \tag{A.9}$$

Using now the steady-state approximation, for holes

$$r_g = k_4'[h^+]_B + k_9[e^-][h^+]_B \tag{A.10}$$

The substitution of (A.10) in (A.9) results in

$$r_e = k_4'[h^+]_B - k_8[O_2]_{ads}[e^-] \tag{A.11}$$

Employing then the steady-state approximation for electrons:

$$[h^+]_B = \frac{k_8}{k_4'}[O_2]_{ads}[e^-] \tag{A.12}$$

and introducing (A.12) into (A.10) a quadratic equation is obtained:

$$r_g = k_8[O_2]_{ads}[e^-] + \frac{k_9 k_8}{k_4'}[O_2]_{ads}[e^-]^2 \tag{A.13}$$

which can be solved for $[e^-]$:

$$[e^-] = \frac{k_4'}{2k_9}\left(1 + \sqrt{1 + \frac{4r_g}{\frac{k_4' k_8}{k_9}[O_2]_{ads}}}\right) \tag{A.14}$$

Now, by introducing (A.14) into (A.12) and rearranging, an expression for $[h^+]_B$ can be written as

$$[h^+]_B = \frac{r_g}{k_4'\left(\frac{1}{2} + \sqrt{\frac{1}{4} + \frac{k_9 r_g}{k_8 k_4'[O_2]_{ads}}}\right)} \tag{A.15}$$

Likewise, from Eqs. (S_0), (S_4), (S_8) and (S_9) of Table 1, the balances for $[h^+]_A$ and $[e^-]$ result as follows:

$$r_{h_A^+} = r_g - k_6[Ox^-]_A[h^+]_A - k_9[h^+]_A[e^-] \tag{A.16}$$

$$r_e = r_g - k_9[h^+]_A[e^-] - k_8[O_2]_{ads}[e^-] \tag{A.17}$$

Using again the steady-state approximation, for $[h^+]_A$ and $[e^-]$:

$$r_g = k_6[Ox^-]_A[h^+]_A + k_9[h^+]_A[e^-] \tag{A.18}$$

$$r_g = k_9[h^+]_A[e^-] + k_8[O_2]_{ads}[e^-] \tag{A.19}$$

and solving for $[h^+]_A$:

$$[h^+]_A = \frac{k_8[O_2]_{ads}[e^-]}{k_6[Ox^-]_A} \tag{A.20}$$

Introducing (A.20) into (A.19), a new quadratic equation is obtained:

$$k_9\frac{k_8[O_2]_{ads}[e^-]^2}{k_6[Ox^-]_A} + k_8[O_2]_{ads}[e^-] - r_g = 0 \tag{A.21}$$

which can be solved for $[e^-]$:

$$[e^-] = \frac{k_6}{2k_9}[Ox^-]_A\left[1 + \sqrt{1 + \frac{4k_9 r_g}{k_6 k_8[O_2]_{ads}}}\right] \tag{A.22}$$

Next, introducing (A.22) into (A.20) and rearranging, an expression for $[h^+]_A$ can be written as

$$[h^+]_A = \frac{r_g}{k_6[Ox^-]_A\left[\frac{1}{2} + \sqrt{\frac{1}{4} + \frac{k_9 r_g}{k_6 k_8[O_2]_{ads}[Ox^-]_A}}\right]} \tag{A.23}$$

and, by substituting Eqs. (A.7), (A.15) and (A.23) into Eq. (A.1), a first general rate expression for the local (intrinsic), overall reaction rate results:

$$r_{ox} = \frac{k_5\theta(t)[Ox^-]_B r_g}{k_{4\_}\left(\frac{1}{2} + \sqrt{\frac{1}{4} + \frac{k_9 r_g}{k_8 k_4'[O_2]_{ads}}}\right)} + \frac{[1 - \theta(t)]r_g}{\frac{1}{2} + \sqrt{\frac{1}{4} + \frac{k_9 r_g}{k_6 k_8[O_2]_{ads}[Ox^-]_A}}} \tag{A.24}$$

On the other hand, since the relevant reactions in the proposed mechanism are heterogeneous processes occurring on the surface of the photocatalytic composite, it is of interest to cast the reaction rate in terms of the relevant parameters of the fluidized bed. The local specific volumetric area of the active catalytic surface (S_v) in the segregated FB can be expressed as a function of the catalyst particle size (D_p), the catalyst density (ρ_c), and either the local catalyst concentration (W_c) or the fluidized bed voidage (ε_h) by assuming spheroid particles for the titania-quartz sand composite composite, as follows:

$$S_V = \frac{6\phi}{\rho_C D_p}W_c = \frac{\varphi(1 - \varepsilon_h)}{D_p} \quad \text{where} \quad \phi' = 6\phi \text{ and } S_V[=]m^2\,m^{-3} \tag{A.25}$$

where ϕ is the sphericity factor of the particles.

And consequently, all the reaction kinetic constants in Eq. (A.24) can be rearranged as

$$k_5 = k_5^0(S_V) = k_5^0\frac{\phi'(1 - \varepsilon_h)}{D_p} \quad \text{where} \quad k_5^0[=]mol^{-1}\,m^2\,s^{-1} \tag{A.26}$$

$$k_6 = k_6^0(S_V) = k_6^0\frac{\phi'(1 - \varepsilon_h)}{D_p} \quad \text{where} \quad k_6^0[=]mol^{-1}\,m^2\,s^{-1} \tag{A.27}$$

$$k_8 = k_8^0(S_V) = k_8^0\frac{\phi'(1 - \varepsilon_h)}{D_p} \quad \text{where} \quad k_8^0[=]mol^{-1}\,m^2\,s^{-1} \tag{A.28}$$

$$k_9 = k_9^0(S_V) = k_9^0\frac{\phi'(1 - \varepsilon_h)}{D_p} \quad \text{where} \quad k_9^0[=]mol^{-1}\,m^2\,s^{-1} \tag{A.29}$$

$$k_4' = k_4'^0(S_V) = k_4'^0\frac{\phi'(1 - \varepsilon_h)}{D_p} \quad \text{where} \quad k_4'^0[=]s^{-1} \tag{A.30}$$

$$\frac{k_9}{k_8 k_4'} = \frac{k_9^0}{k_8^0 k_4'^0}(S_V)^{-1} = \frac{k_9^0 D_p}{k_8^0 k_4'^0 \phi'(1-\varepsilon_h)} \quad \text{where} \quad \left[\frac{k_9^0}{k_8^0 k_4'^0}\right][=]\text{s} \qquad (A.31)$$

$$\frac{k_9}{k_8 k_6} = \frac{k_9^0}{k_8^0 k_6^0}(S_V)^{-1} = \frac{k_9^0 D_p}{k_8^0 k_6^0 \phi'(1-\varepsilon_h)} \quad \text{where} \quad \left[\frac{k_9^0}{k_8^0 k_6^0}\right][=]\,\text{mol m}^{-2}\,\text{s} \qquad (A.32)$$

Hence, by introducing Eqs. (A.25)–(A.32) into Eq. (A.24), the latter can be written as

$$r_{ox} = \frac{k_B \theta(t)[Ox^-]_B r_g}{\frac{1}{2} + \sqrt{\frac{1}{4} + \frac{k_B' D_p r_g}{\phi'(1-\varepsilon_h)[O_2]_{ads}}}} + \frac{[1-\theta(t)] r_g}{\frac{1}{2} + \sqrt{\frac{1}{4} + \frac{D_p k_A r_g}{\phi'(1-\varepsilon_h)[O_2]_{ads}[Ox^-]_A}}} \qquad (A.33)$$

where

$$k_B = \frac{k_5^0}{k_4^0}; \quad k_B' = \frac{k_9^0}{k_8^0 k_4'^0}; \quad \text{and} \quad k_A = \frac{k_9^0}{k_6^0 k_8^0}$$

Appendix B. Calculation procedure

(i) The oxalic acid concentrations in the recirculating tank, $[Ox]_{Tk}$, and the FB reactor, $[Ox]_R$, are initialized at zero time (t=0). Prior to the removal of the lamp shutters the solution recirculates 'in the dark'. Therefore, both initial concentrations are equal to the concentration of oxalic acid introduced into the system, $[Ox^-]_R^0$, $[Ox^-]_{Tk}^0 = [Ox^-]_{sol}^0$, $t=0$. (ii) A first time increment is introduced (i.e.: t becomes equal to $t+\Delta t$). (iii) The mass balance in the tank is then solved for a time period between $t-\Delta t$ and t. The incoming concentration to the tank at $t-\Delta t$ (which is equal to the outgoing reactor concentration) is taken as the initial condition. In this step, the concentration at the tank exit is at time t is obtained. (iv) The material balance in the reactor is solved at time t, by utilizing as the inward reactor concentration the outgoing tank concentration obtained in the previous step (step iii). The concentration profile and, as a result, the outgoing concentration for the reactor at time t is obtained in this step. At each time step the previous concentration profile in the reactor at time $t-\Delta t$ is required. (v) If the 'elapsed time' t were less than the total run time the concentrations set must be updated. The former concentrations are replaced by the 'present' concentrations at the new time increment and the 'former' concentration profile inside the reactor is the one that had been calculated in step (iv); the calculation process goes back to step (ii), and so on. Otherwise, the calculation procedure is finished.

This calculation scheme is straightforward whenever the kinetic parameters are known in advance. Since this is not our case, a non-linear least-squares regression routine for parameters estimation was used to determine the parameter values that minimize the sum of the quadratic differences between the experimental and model obtained concentrations. The complete set of experimental data was employed.

References

Al-Ekabi, H., Serpone, N., 1988. Kinetic studies in heterogeneous photocatalysis. Journal of Physical Chemistry 67, 109–115.

Alfano, M., Cabrera, M., Cassano, A., 1997. Photocatalytic reactions involving hydroxyl radical attack. I. Reaction kinetics formulation with explicit photon absorption effects. Journal of Catalysis 172, 370–379.

Araujo, P., Mendive, C., García Rodenas, L., Morando, P., Regazzoni, A., Blesa, M., Bahnemann, D., 2005. FT-IR-ATR as a tool to probe photocatalytic interfaces. Colloids and Surfaces A: Physicochemical and Engineering Aspects 265, 73–80.

Bahnemann, D., Hilgendorff, M., Memming, R., 1997. Charge carrier dynamics at TiO_2 particles: reactivity of free and trapped holes. Journal of Physical Chemistry 101, 4265–4275.

Bahnemann, D., 1999. Photocatalytic detoxification of polluted waters. In: Boule (Ed.), The Handbook of Environmental Chemistry, vol. 2, Part L. Springer, Berlin, Heidelberg, pp. 285.

Blanco, J., Malato, S., Estrada, C., Bandala, E., Gelover, S., Leal, T., 2001. Purificación de Aguas por Fotocatálisis Heterogénea: Estado del Arte. In: Blesa, M. (Ed.), Eliminación de Contaminantes por Fotocatálisis Heterogénea, ISBN: 987-43-3809-1. Cap. 3, Red CYTED VIII-G, Argentina, p. 51.

Choi, W., Hoffmann, M.R., 1995. Photoreductive mechanism of CCl_4 degradation on TiO_2 particles and effects of electron donors. Environmental Science &Technology 29, 1646–1654.

Hug, S., Sulzberger, B., 1994. In-situ Fourier transform infrared spectroscopic evidence for the formation of several different surface complexes of oxalate on TiO_2 in the aqueous phase. Langmuir 10, 3587–3597.

Imoberdorf, G.E., Irazoqui, H.A., Alfano, O.M., Cassano, A.E., 2007. Scaling-up from first principles of a photocatalytic reactor for air pollution remediation. Chemical Engineering Science 62, 793–804.

Jiang, D., Zhao, H., Zhang, S., John, R., 2004. Kinetic study of photocatalytic oxidation of adsorbed carboxylic acids at TiO_2 porous films by photoelectrolysis. Journal of Catalysis 223 (1), 212–220.

Kosanić, M.M., 1998. Photocatalytic degradation of oxalic acid over TiO_2 powder. Journal of Photochemistry and Photobiology A: Chemistry 119 (4), 119–122.

Krýsa, J., Waldner, G., Měšťánková, H., Jirkovsky, J., Grabner, G., 2006. Photocatalytic degradation of model organic pollutants on an immobilized particulate TiO_2 layer. Roles of adsorption process and mechanistic complexity. Applied Catalysis B. Environmental 64, 290–301.

Mao, Y., Schöneich, C., Klauss-Dieter, A., 1991. Identification of organic acids and other intermediates in oxidation degradation of chlorinated ethanes on TiO_2 surfaces en route to mineralization. A combined photocatalytic and radiation chemical study. Journal of Physical Chemistry 95, 10080–10089.

Matthews, R., 1987. Adsorption photocatalytic oxidation: a new method of water photooxidation of organic impurities in water using thin films of titanium dioxide. Journal of Physical Chemistry 91 (12), 3328–3333.

Mendive, C., Bahnemann, D., Blesa, M., 2005. Microscopic characterization of the photocatalytic oxidation of oxalic acid adsorbed onto TiO_2 by FTIR-ATR. Catalysis Today 101 (3), 237–244.

Mendive, C., Bredow, T., Blesa, M., Bahnemann, D., 2006. ATR-FTIR measurements and quantum chemical calculations concerning the adsorption and photoreaction of oxalic acid on TiO_2. Physical Chemistry Chemical Physics 8, 3232–3247.

Mendive, C., Bredow, T., Blesa, M., Bahnemann, D., 2007. The adsorption and photodegradation of oxalic acid at the TiO_2 surface. Water Science & Technology. 55 (12), 139–145.

Morstein, M., Karches, M., Pozzo, R.L., Giombi, J.L., Baltanás, M.A., 2002. Plasma-CVD-coated glass beads as photocatalyst for water decontamination. Catalysis Today 72, 267–279.

Nikov, I., Karamazov, D., 1991. Liquid–solid mass transfer in inverse fluidized bed. A.I.Ch.E. Journal 37 (9), 781–784.

Peill, N.J., Hoffman, M.R., 1996. Chemical and physical characterization of a TiO_2-coated fiber optic cable reactor. Environmental Science & Technology 30, 2806–2812.

Pozzo, R.L., Baltanás, M.A., Cassano, A.E., 1999. Towards a precise assessment of the performance of supported photocatalysts for water detoxification process. Catalysis Today 54 (1), 143–157.

Pozzo, R.L., Brandi, R.J., Giombi, J.L., Baltanás, M.A., Cassano, A.E., 2005. Design of fluidized bed photoreactors: optical properties of photocatalytic composites of titania CVD-coated onto quartz sand. Chemical Engineering Science 60, 2785–2794.

Pozzo, R.L., Brandi, R.J., Giombi, J.L., Cassano, A.E., Baltanás, M.A., 2006. Fluidized bed photoreactors using composites of titania CVD-coated onto quartz sand as photocatalyst: assessment of photochemical efficiency. Chemical Engineering Journal 118, 153–159.

Sabate, J., Anderson, M.A., Kikkawa, H., Edwards, M., Hill Jr., C.G., 1991. A kinetic study of the photocatalytic degradation of 3-chlorosalicylic acid over TiO_2 membranes supported on glass. Journal of Catalysis 127, 167–177.

Turchi, C.S., Ollis, D.F., 1990. Photocatalytic degradation of organic water contaminants: mechanisms involving hydroxyl radical attack. Journal of Catalysis 122, 178–192.

Weisz, A., Regazzoni, A., Blesa, M., 2001. ATR-FTIR study of the stability trends of carboxylate complexes formed on the surface of titanium dioxide particles immersed in water. Solid State Ionics 143, 125–130.

Zalazar, C.S., Romero, R.L., Martín, C.A., Cassano, A.E., 2005. Photocatalytic intrinsic reaction kinetics I: mineralization of dichloroacetic acid. Chemical Engineering Science 60 (19), 5240–5254.